Numerical Simulation of the Atmospheric Response to Equatorial Pacific Sea Surface Temperature Anomalies

J. SHUKLA

Laboratory for Atmospheric Sciences, NASA/Goddard Space Flight Center, Greenbelt, MD 20771

J. M. WALLACE

Department of Atmospheric Sciences, University of Washington, Seattle, WA 98195

(Manuscript received 4 November 1982, in final form 22 March 1983)

ABSTRACT

A number of recent observational and theoretical studies indicate that under certain conditions tropical sea surface temperature anomalies may be capable of producing climatic anomalies at extratropical latitudes. According to the hypothesis put forth in these studies, perturbations in the climatological mean distribution of precipitation in the tropics can influence the extratropical circulation through the action of forced, quasi-stationary, two-dimensional, Rossby wavetrains, which may tend to excite the fastest growing normal mode associated with barotropic instability.

Results of previous GCM experiments designed to simulate the atmospheric response to SST anomalies are re-examined in light of this hypothesis and are found to be generally consistent with it.

A modeling investigation consisting of three separate GCM experiments was carried out using the GLAS climate model with January initial conditions based on observed data and an equatorial Pacific sea surface temperature anomaly based on the recent analysis of Rasmusson and Carpenter (1982).

The observed eastward shift of the belt of heavy convective precipitation in the western Pacific during the episodes of positive sea surface temperature anomalies was correctly simulated in all three experiments. Associated with this, the ascending branch of the Walker circulation also shifted eastward and the north–south overturning intensified in the central Pacific. The 300 mb height difference field, averaged for the three pairs of experiments, showed evidence of two-dimensional Rossby wave propagation along a great circle path, poleward over the North Pacific and eastward across the North Pacific, in agreement with observations and with the results of experiments with simpler models. However, there was considerable variability from experiment to experiment and there were unexpected features over Eurasia in the average difference pattern. As in previous experiments, the simulations with sea surface temperature anomaly produced an increase of low-level westerlies along the equator, slightly to the west of the enhanced rainfall. It was the moisture convergence, associated with the anomalous low-level circulation rather than the local changes in evaporation, which accounted for most of the simulated changes in precipitation. The simulated circulation changes at extratropical latitudes exhibited an equivalent barotropic vertical structure, in agreement with observations. The sea level pressure associated with warm sea surface temperature anomalies was lower over the eastern Pacific and higher over the western Pacific and the Indian Ocean in agreement with the observed Southern Oscillation.

1. Introduction

There exists a growing body of observational and modeling evidence to the effect that sea surface temperature (SST) anomalies in the equatorial Pacific exert a significant influence upon wintertime climate in the Pacific/North American sector of the hemisphere. The sequence of mechanisms through which this influence is believed to occur is as follows:

1) Large-scale, coupled, atmosphere-ocean interactions in the tropical Pacific, whose workings are not yet fully understood, result in prolonged episodes during which the normally cold equatorial surface waters in the eastern half of the Pacific are several degrees warmer than normal. The characteristic life cycle of these warm episodes is documented in a recent paper by Rasmusson and Carpenter (1982). Fig. 1, which is derived from their paper, shows the pattern of SST anomalies during what they refer to as the "mature phase" of these warm episodes, which corresponds to the Northern Hemisphere winter following almost a year after the first appearance of the warm water along the coast of Peru and Ecuador. It can be seen that at this time the anomalies are largest in the eastern Pacific, between 100 and 160°W, but significant anomalies extend all the way westward to near 160°E.

2) During the mature phase of these warm episodes, the SST pattern is distorted such that warm (>29°C) water extends eastward along the equator to near the Line Islands, ~160°W, whereas, during more typical Northern Hemisphere winters, such

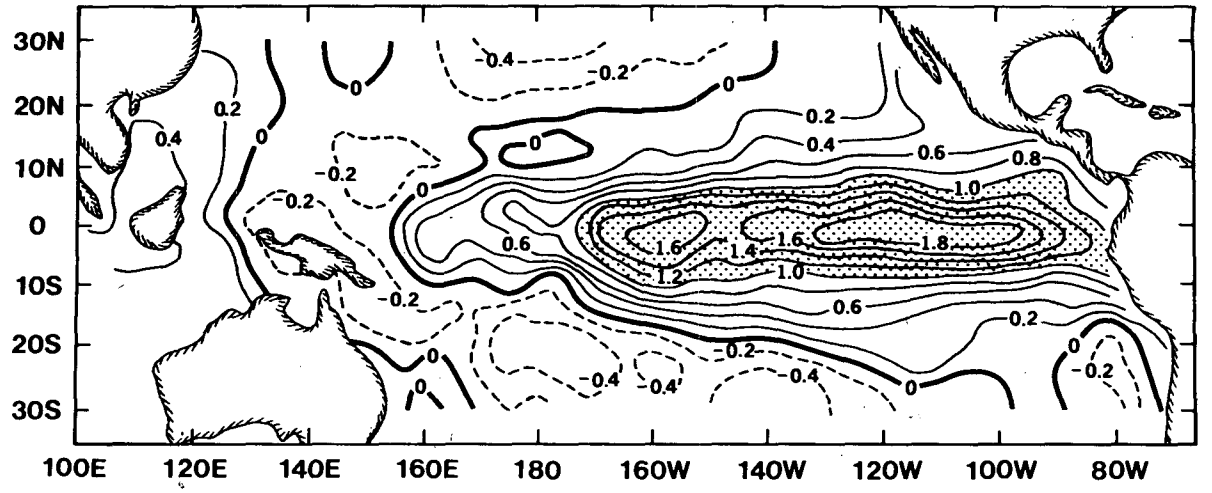

FIG. 1. Observed sea surface temperature anomaly for the months of November, December, and January averaged for the years 1957–58, 1965–66, 1969–70 and 1972–73 (after Rasmusson and Carpenter, 1982).

warm waters are found only to the west of the dateline. These differences are evident in Fig. 2, which shows the normal January SST climatology contrasted against a "warm episode January climatology" derived by adding the anomaly field in Fig. 1 to the normal January climatology.

3) The region of deep cumulus convection which is normally confined to the extreme western Pacific shifts eastward with the warm water. Doberitz (1968), Bjerknes (1969) and others have shown that precipitation at equatorial island stations in the vicinity of the dateline increases from near zero during normal Januaries to amounts on the order of 15 mm day^{-1} during Januaries which fall within the warm episodes. The region of sharply enhanced rainfall, as deduced from satellite imagery during the two most recent warm episodes by Rao and Theon (1977), Heddinghaus and Kreuger (1981), Liebmann and Hartmann (1982) and Lau and Chan (1983), is indicated by the shading in Fig. 3. During these same Januaries, precipitation is abnormally light in the extreme western Pacific, Indonesia, and northern Australia (Quinn *et al.*, 1978; Pittock, 1973; Kidson, 1975).

4) These changes in the pattern of precipitation at equatorial latitudes are reflected in the pattern of upper level (~200 mb) divergence which, in turn, in-

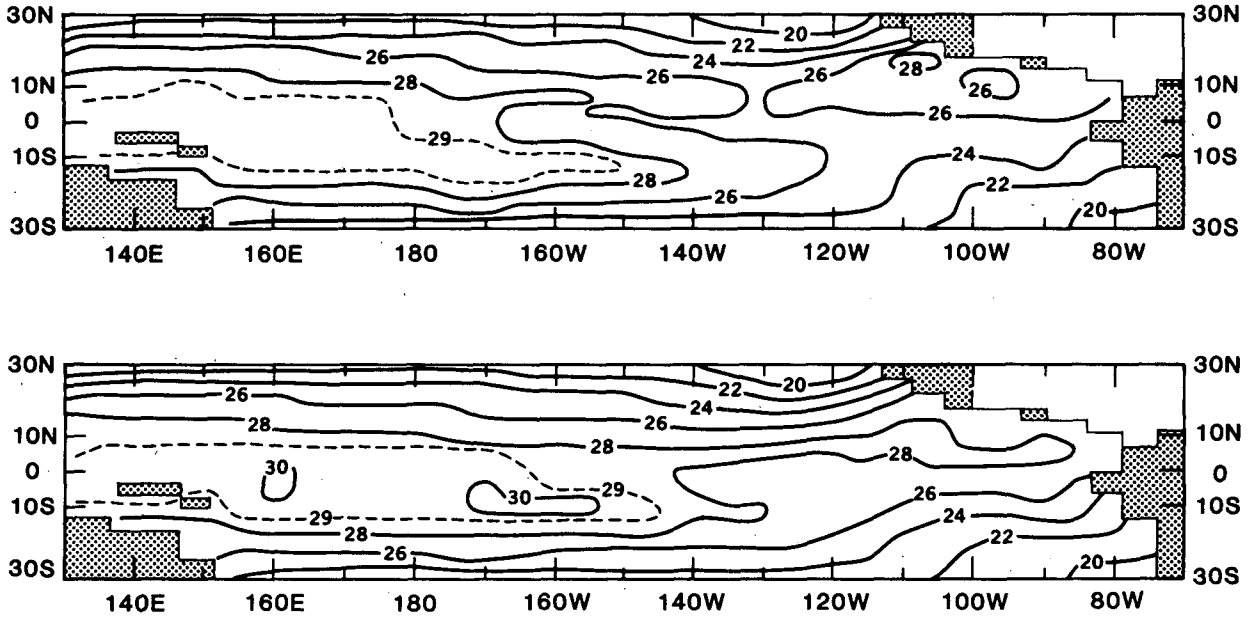

FIG. 2. Climatological mean sea surface temperature over Pacific during January (a) control case, (b) anomaly case obtained by addition of the fields in Figs. 1 and 2a.

fluences the stationary wave pattern at extratropical latitudes in the Northern Hemisphere. The resulting stationary wave perturbations, illustrated schematically in Fig. 3a have been interpreted in terms of Rossby-wave dispersion on a sphere from a localized vorticity source on the equator (Hoskins and Karoly, 1981; Opsteegh and van den Dool, 1980; Horel and Wallace, 1981; Webster, 1981; for a review of the relevant theoretical background see Hoskins, 1983). Alternatively, Simmons *et al.* (1983) have suggested that these same stationary wave perturbations can be identified with the fastest growing mode associated with barotropic instability of the climatological upper level mean wintertime flow, which can be excited in a variety of ways: perturbations with the observed polarity can be generated by a source of upper level divergence over the central Pacific or (even more effectively) by convergence (such as might be associated with decreased rainfall) over the extreme western Pacific, Indonesia, and the South China Sea.

5) In the region where the redistribution of rainfall takes place, the perturbations in divergence in the lower troposphere are opposite in polarity to those in the upper troposphere (e.g., there is increased low-level convergence in the region near the dateline where the rainfall increases during the warm episodes). The resulting low level wind perturbations, described schematically in Fig. 3b, are in accord with theoretical results of Webster (1981, 1982) who considered the response of a two-layer primitive equation model atmosphere to localized SST anomalies at various latitudes on a spherical earth. At tropical latitudes the simulated perturbations are of opposite polarity at upper and lower levels and their horizontal structure is consistent with solutions obtained by Matsuno (1966) and Gill (1980) using equatorial beta plane geometry. At higher latitudes, the observed perturbations assume an equivalent barotropic vertical structure with the same polarity throughout the troposphere. The amplitude of the perturbations increases from lower to upper troposphere, so that temperature and geopotential height tend to be in phase. Thus, for example, during the winters which fall within the warm episodes, temperatures tend to be above normal in western Canada and below normal in the southeastern United States. The equivalent barotropic vertical structure of the perturbations outside of the immediate region of the forcing is successfully simulated in the two-layer primitive equation models of Webster (1981) and Opsteegh and van den Dool (1980) and in the five-layer model of Hoskins and Karoly (1981).

Hence, there now exists the elements of a dynamical framework for interpreting the observed relationships between equatorial sea surface temperatures and wintertime climatic anomalies in extratropical latitudes. Experiments with the hierarchy of simple

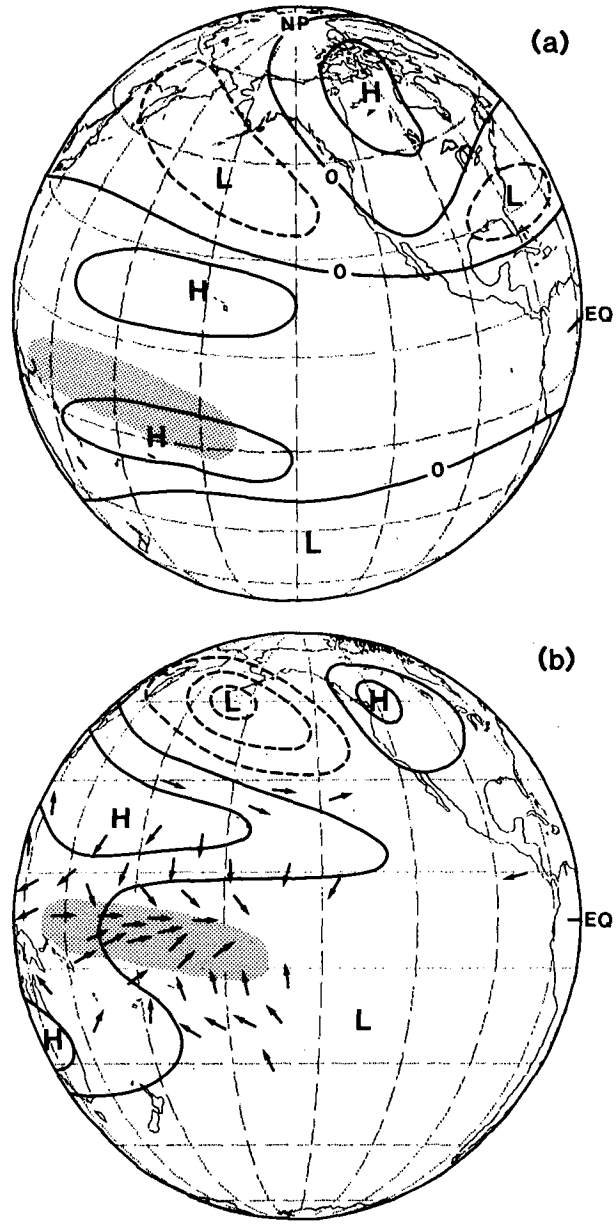

FIG. 3. Schematic representation of teleconnection patterns associated with the equatorial sea-surface temperature anomalies shown in Fig. 1. (a) upper tropospheric geopotential height, (b) sea-level pressure and surface wind. Shading denotes region of enhanced rainfall.

models alluded to above have had considerable success in simulating the three-dimensional structure and seasonal dependence of the observed climatic anomalies. It remains to be seen whether more comprehensive and detailed models will be capable of producing a quantitative simulation of these relationships.

General circulation models (GCMs) include explicit representation of a number of potentially im-

TABLE 1. Tropical sea surface temperature anomaly experiments.

Investigator(s)/model	Design of experiments
(a) *Equatorial Pacific anomalies*	
Rowntree (1972): GFDL 9-level primitive equation model with equatorial "wall." N20 version with 320–640 km horizontal resolution. Perpetual January conditions.	Control and anomaly runs starting from observed conditions for two January days in different years. SST anomaly shown in Fig. 4a. Auxiliary experiments with halved anomaly and phase shifted (by 60° longitude) anomaly. Analysis based on averages for days 21–30 of the integrations.
Julian and Chervin (1978): NCAR 6-level global primitive equation model with 5° latitude × 5° longitude grid. Perpetual January conditions.	Control and anomaly experiments starting with isothermal atmosphere at rest and integrated for 60 days, anomaly experiments based on two different anomaly fields: one of which is shown in Fig. 4b. Analysis based on averages for days 31–60 of integrations. Additional experiment to determine response time.
Keshavamurty (1982): GFDL 9-level, global, spectral, primitive-equation model with rhomboidal 15 truncation. Seasonal cycle.	The control experiment is a 15 year simulation for which seasonal averaged (June–August) climatology has been documented. Five anomaly experiments were carried out: two for an eastern Pacific anomaly, two for a central Pacific anomaly, and one for a western Pacific anomaly. The SST anomalies are shown in Fig. 4c. Each anomaly experiment was run for 5½ months, beginning with the insertion of the SST anomaly into model data for 16 March from one of the years of the control experiment. Analysis is based on 90 day (June–August) averages.
Shukla and Wallace (1983, *loc. cit.*): NASA/GLAS 9-level, global, grid point, primitive-equation model with 4° latitude × 5° longitude resolution. Seasonal cycle.	Three pairs of control/anomaly experiments based on the SST anomaly shown in Figs. 1 and 4d. The initial conditions for the three experiments were the observed NMC analysis for 1 Jan 1975, 1 Jan 1977 and the model simulation at the end of 31 days starting with 1 Jan 1975. Analysis is based on first 60 days of first two pairs and 30 days of third pair of integrations.
(b) *Other tropical SST anomalies*	
Rowntree (1976): Same model as in Rowntree (1972).	Experiments based on subtropical anomaly shown in Fig. 4e. Five control experiments started from various initial conditions; three anomaly experiments. An additional integration based on an equatorial Atlantic anomaly. Analysis based on averages for days 41–80.
Shukla (1975): GFDL 11-level global primitive equation model with 2.5° latitude × 2.5° longitude grid.	Experiment based on Arabian Sea anomaly shown in Fig. 4f. One control run started from day 1261 of seasonal cycle run corresponding to 15 June and one anomaly run for the period 15 June–1 August. Results were analyzed for July mean.
Moura and Shukla (1981): Same model as Shukla and Wallace (1982).	Experiments based on tropical Atlantic anomaly shown in Fig. 4f. One control and one anomaly run starting from observed initial conditions of 1 Jan, 1975 (NMC analysis). Analysis based on first 60 days of integration.

portant dynamical processes which are ignored or are only crudely parameterized in the simplified models discussed above:

1) Parameterization of boundary layer processes and moist convection, by which the imposed SST anomaly interacts with the dynamics to produce a tropical heating anomaly. The structure of the large scale flow determines whether a SST anomaly will produce a deep heat source. In most of the simplified models alluded to above, the heating anomaly is prescribed directly. (The one exception is the two-layer model of Webster which incorporates an iterative scheme to determine the total diabatic heating that would result from an initial heating field directly related to the prescribed SST anomaly.)

2) Planetary wave propagation in the vertical. In the one and two layer models the vertical structure of the background flow and the waves is not adequately resolved to permit an accurate quantitative determination of the three-dimensional dispersion of the planetary waves induced by the SST anomalies.

3) Nonlinear interactions between the induced perturbations and the background flow, particularly in the tropics, where there is the likelihood of important feedbacks. Changes in the background flow can affect the propagation properties.

4) Feedbacks involving transient fluctuations associated with baroclinic instability at higher latitudes.

5) The nonlinear feedback of the perturbations induced by the SST anomalies upon the forcing of the climatological mean stationary waves; e.g., if the

flow over the Rockies is changed by the presence of the SST anomalies, then the orographic forcing for the planetary waves is correspondingly changed. Midlatitude flow can be changed either by changes in the north–south overturnings (Hadley type) or wave patterns forced by SST anomalies.

Furthermore, in a GCM simulation it is possible to take into account the fact that the prescribed SST anomalies are superimposed upon a climatological mean SST distribution which already contains strong longitudinal structure. It will presently be shown that the presence of this background field, which is ignored in the simplified models, strongly influences the character of the tropical response to the SST anomalies in the Pacific.

2. Review of previous GCM experiments

Several general circulation model (GCM) experiments have already been carried out for the purpose of investigating the influence of tropical SST anomalies upon the planetary-scale atmospheric circulation. Some of the major experiments, including the ones in the present study, are summarized in Table 1 and Fig. 4. In Table 1, the experiments based on equatorial Pacific SST anomalies are grouped separately from the others and described in somewhat more detail.

With the possible exception of the study of Keshavamurty (1982), these experiments were designed, and the results from them were analyzed without the benefit of the conceptual framework described in Section 1, which might have served as a hypothesis to be tested and as a framework for organizing and comparing the results. Nevertheless, it is possible, in retrospect, to extract from the results of these experiments, consistent evidence to the effect that SST anomalies alter the distribution of tropical precipitation, and that these changes in precipitation, in turn, can influence the extratropical circulation by changing the zonal flow and through two-dimensional Rossby-wave propagation:

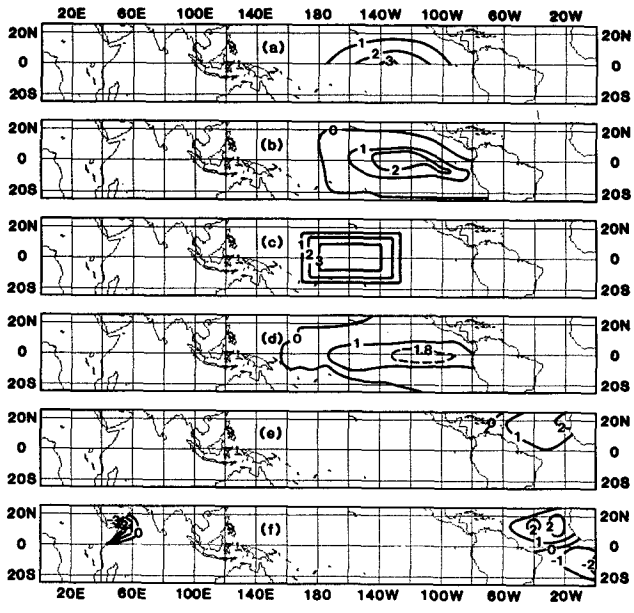

FIG. 4. Sea surface temperature anomalies used in GCM sensitivity experiments: (a) Rowntree (1972), (b) Julian and Chervin (1978), (c) Keshavamurty (1982), (d) the present study, (e) Rowntree (1976), (f) Shukla (1975) for the Arabian sea, and Moura and Shukla (1981) for the Atlantic.

1) All the studies cited in Table 1a concluded that variations in tropical sea surface temperature, of a realistic magnitude and spatial scale, are capable of producing a significant atmospheric response, which involves changes in the distribution of tropical precipitation.

2) The three studies based on SST anomalies in the equatorial Pacific all reported changes in rainfall qualitatively consistent with Fig. 3 to the extent that they can be compared. In most of the individual experiments, the largest increases in precipitation occurred somewhat to the west of the largest SST anomalies. Rowntree (1972) and Keshavamurty (1982), in his "Central Pacific Anomaly Experiment," (the most relevant one for comparison here) noted decreases in precipitation in the extreme western Pacific.

3) In all the experiments with equatorial SST anomalies, there was a consistent pattern of changes in the upper level flow in the tropics and subtropics: (i) the flow over the equator became more easterly over and to the west of the region of enhanced precipitation, (ii) anticyclonic circulation anomalies developed at latitudes near 20°N at the longitude of the anomalous equatorial easterlies, and (iii) further poleward near 35° latitude there was a tendency for an enhancement of the westerly jetstreams at these longitudes. These circulation changes are in accord with Fig. 3a.

4) In the results of Rowntree (1972) and Keshavamurty (1982), there was evidence of changes in the upper tropospheric wind field consistent with the notion of wavetrains oriented along great circle routes. Rowntree's pattern bears a direct resemblance to Fig. 3a. Keshavamurty's extratropical response was mainly in the Southern Hemisphere (the winter hemisphere for his experiment), in agreement with theoretical expectations. Although Julian and Chervin's (1978) extratropical response did not appear to be statistically significant according to the *t*-test, the pattern of response is in general agreement with the other results with the exception of an eastward shift.

5) In all three of his experiments, Keshavamurty reported an increase in low-level westerlies along the equator to the west of the region of enhanced precipitation, in agreement with Fig. 3b. [Rowntree (1972) did not show low-level wind fields and Julian

and Chervin did not find evidence of statistically significant low-level wind changes along the equator.]

6) In Julian and Chervin's experiments and in Keshavamurty's "Central Pacific Anomaly Experiment," there was evidence of increases in the low-level tradewind flow at 15–20°N latitude as in Fig. 3b. In the former experiments, these changes were primarily over the eastern half of the Pacific, whereas in the latter experiment, they were primarily in the western half.

7) The vertical structure of the extratropical circulation anomalies is not extensively discussed in any of these papers, but from fragmentary evidence presented in the figures it can be inferred that it is primarily equivalent barotropic, as in Fig. 3, with temperature anomalies and geopotential height anomalies occurring in phase with one another in the lower troposphere. For example, in both Rowntree's anomaly experiments, warm ridges developed over western Canada.

We do not expect the model results to be identical because different models can produce different types of precipitation anomalies and mean flows, which in turn can produce different responses in the tropical and extratropical latitudes. However, in spite of substantial differences in the models and SST anomaly patterns used by Rowntree, Julian and Chervin (they used one realistic and one "superanomaly" pattern), and Keshavamurty, the results of prior GCM simulations, to the extent they can be compared, lend additional support to the conceptual model summarized in Section 1. Unfortunately, of the previous GCM experiments, the one by Keshavamurty is the only one for which results are presented in a way that can be compared with Fig. 3. However, Keshavamurty's experiments were based on July, rather than January conditions (the emphasis being on the interaction with the Asian summertime monsoon), and his SST anomaly fields were narrower in longitudinal extent, wider in meridional extent, and somewhat larger in amplitude than the observed ones.

3. Plan of the present study

The emergence of a more definitive observational basis for designing GCM experiments to investigate the atmospheric response to equatorial SST anomalies and a clearer theoretical framework for interpreting the results of such experiments prompted the WMO/CAS[1] Working Group on Numerical Experimentation (WGNE) to recommend a series of GCM experiments to be conducted by a number of different modeling groups, in order to determine the atmospheric response to a single "standard" distribution of equatorial Pacific SST anomalies; namely, the one shown in Fig. 1 of this paper.

The present study, which is based on that same anomaly field, was already in progress at the time that the WGNE recommendation was made. It involves a series of extended (1–2 month) integrations, each consisting of a control run (C) based on the normal January SST climatology shown in Fig. 2a and an anomaly run (A) based on the perturbed SST anomaly shown in Fig. 2b. The first pair of integrations, denoted by C_1 and A_1 were started from observed initial conditions for 1 January 1975, and the second pair (C_2 and A_2) from 1 January 1977. Both pairs of integrations were run for two months (60 days). An additional integration was carried out starting from initial conditions on day 31 of the first control run, C_1. This run, which was terminated at the end of the first month (day 30), is denoted by A_3. Results were analyzed separately for each month of the integrations, where the month (1 or 2) is indicated by a second subscript on the identifier; for example, C_{21} refers to the first month of the second control run (see Table 2). Results for the first month are averaged for days 11–30 instead of the full month in order to allow sufficient time for the model physics to produce precipitation anomalies and for the hypothesized Rossby wave pattern to develop in response to the heating anomalies associated with the enhanced precipitation.

For some selected fields we have also shown a 15 day average (days 11–25) for C_{11} which had the most pronounced change in the rainfall and other circulation features. The main motivation for presenting short period results is to show an example of a rapid model response to SST anomalies. These results may have important implications for the use of this or similar models for dynamical prediction of monthly means using climatological or observed SST boundary conditions.

4. The GLAS climate model

The general circulation model and its simulation of the winter and summer circulation has been described by Shukla *et al.* (1981). It is a global model

TABLE 2. List of model experiments and notation for different averaging periods.

Initial conditions	Averaging periods: Days 11–30 Control	Days 11–30 Anomaly	Days 31–60 Control	Days 31–60 Anomaly
1 January 75	C_{11}	A_{11}	C_{12}	A_{12}
1 January 77	C_{21}	A_{21}	C_{22}	A_{22}
Day 31 of C_{11}	C_{31}	A_{31}	—	—

(Differences $D_{ij} = A_{ij} - C_{ij}$)

[1] World Meteorological Organization/Committee for Atmospheric Sciences.

with nine layers of equal sigma coordinate thickness in vertical and a 4° × 5° latitude–longitude grid in horizontal. The upper boundary is at 10 mb and the top layer is centered at ~65 mb. The number of grid points is systematically reduced near the poles such that the longitudinal grid length along a latitude circle is 10° in longitude between latitudes 66 and 78°, and 20° in longitude between 82 and 90°. A sixteenth-order Shapiro filter is applied once every simulated half hour in the longitudinal direction to the sea level pressure, potential temperature, and wind components. For time integration, the Matsuno forward–backward time differencing scheme is used. Clouds are predicted by the model parameterizations of cumulus convection and large-scale saturation. The cumulus parameterization scheme includes rainfall due to low, medium and deep convective clouds which are confined to the lowest six layers, and supersaturation clouds which can occur in any of the nine layers. These four types of clouds are generated sequentially. First the mid-level, then deep, and then the low-level cumulus clouds are generated, which are followed by generation of supersaturation clouds. Each cloud modifies the environment at its sigma level and, therefore, affects the onset of subsequent clouds in the sequence. A cumulus cloud appears between two levels if the moist static energy at the cloud base exceeds the saturation moist static energy at its top. The supersaturation cloud can appear at any level if the specific humidity at that level exceeds the saturation specific humidity. Rain falling through a dry layer is allowed to evaporate. The longwave radiation calculation is done every 5 h, and the shortwave radiation calculation is done every 30 min. The dynamically generated clouds vary continuously in space and time and affect the shortwave and longwave radiation fluxes. For calculation of absorption of solar radiation within a given cloud layer, the solar optical thickness is prescribed depending on cloud type and cloud level. For longwave radiation, if a cloud appears at any grid point, irrespective of its height and type, it is considered as a black body covering the entire horizontal area of the grid element. The heat exchanges at the lower boundary take place through sensible and latent heat fluxes which depend upon the surface wind, static stability, and vertical gradients of temperature and moisture. The ground temperature is determined by a balance among all the incoming and outgoing heat fluxes, and the changes in the soil moisture are determined by a simple ground hydrology model which accounts for the rainfall, evapotranspiration, and runoff at each land grid point. Climatological monthly mean sea-surface temperatures are used to interpolate their daily values over the ocean grid points. The surface albedoes are prescribed for the land, ocean, and desert grid points. The initial soil moisture is obtained from climatological surface air relative humidities.

Shukla *et al.* (1981) have presented a detailed description of the winter and summer simulations, and the reader is referred to this report for more information on the abilities and limitations of this model for climate simulation. We mention here salient features only. The model produces realistic simulations of the global distributions of sea level pressure, wind and precipitation. The model simulated stationary wave variance and the structure and magnitudes of the cyclone scale variance are in agreement with the observed climatological variances. The model shows excessive cooling at the upper levels near the poles. The low-frequency planetary wave variances are underestimated but have the correct latitude–height structure. The simulation of the mean fields for the Southern Hemisphere is also quite reasonable. We will describe some other deficiencies of the model in the later sections of this paper.

5. Results

a. Tropical precipitation

In order to illustrate the effect of the SST anomaly upon the distribution of precipitation we have shown, in a digital format, the distribution of moderate and heavy precipitation averaged for the control runs (Fig. 5a) and the anomaly runs (Fig. 5b). Formally, the average of the anomaly runs is defined as

$$\bar{A} = (20\,A_{11} + 30\,A_{12} + 20\,A_{21} + 30\,A_{22} + 20\,A_{31})/120$$

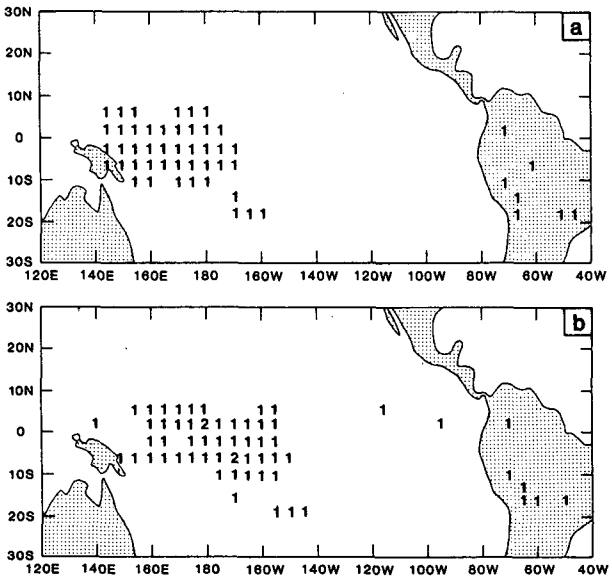

FIG. 5. Average precipitation for (a) control runs $\bar{C}$, (b) anomaly runs $\bar{A}$. Digits 1 and 2 at the model grid points denote precipitation rates of 10–20 mm/day and greater than 20 mm/day, respectively.

or, alternatively,

$$\bar{A} = (50\,A_1 + 50\,A_2 + 20\,A_3)/120,$$

and similarly for the control runs. (Note that days 41–60 are common in C_{12} and C_{31} and therefore are counted twice in computing $\bar{C}$.)

It can be seen that the heavy equatorial precipitation shifts eastward from near 150°E in the control experiments to near the dateline in the anomaly experiments. Figure 6 shows the corresponding distributions for days 11–25 of C_{11} and A_{11}, a period when these changes in the patterns were particularly pronounced. There is some indication of an enhancement of the ITCZ further east in the Pacific in the anomaly experiments which resembles observed changes described by Liebmann and Hartmann (1982) but this is clearly a secondary effect. We will be showing results for this same 15 day period for other selected fields later on in the paper, in order to give an indication of the kinds of conditions that might occur in the model on time scales of a month in association with a strong equatorial precipitation anomaly.

The actual change ($\bar{D} \equiv \bar{A} - \bar{C}$) in precipitation and evaporation in units of mm day^{-1} is shown in Fig. 7. The pattern is dominated by a dipole configuration which reflects the eastward shift of the heaviest precipitation from near 165°E to near the dateline. It is evident from Fig. 8 that this dipole pattern (which, according to the hypothesis put forth in Section 1, may be viewed as the forcing for the large-scale circulation changes in extratropical latitudes) was present in each of the five individual months of the numerical experiments, though not with equal amplitude or in exactly the same position. The change D_{11} has the strongest dipole pattern of all the individual months, with large anomalies in the equatorial belt; the pattern in D_{12} is weaker and largely confined to the Southern Hemisphere; D_{21} has a strong pattern in the equatorial belt, but the longitudinal separation between the centers of the dipole is only about 20° (versus 35° for D_{11}); D_{22} has one of the stronger patterns which spans the equatorial belt and has about a 30° longitudinal separation between centers, and D_{31} resembles D_{12} except that the equatorial portion of the signal is much stronger. Several of the individual months show indications of an enhancement of precipitation along the ITCZ to the east of the dateline, with D_{11} showing the largest changes.

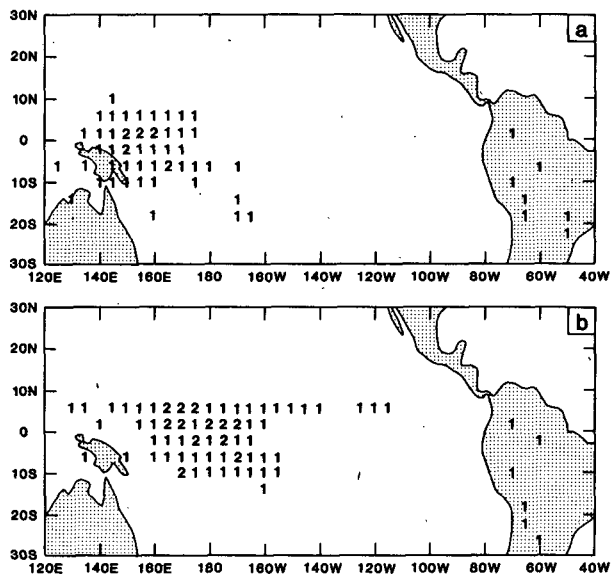

FIG. 6. As in Fig. 5 but for averaging period days 11–25. (a) control run C_{11}, (b) anomaly run A_{11}.

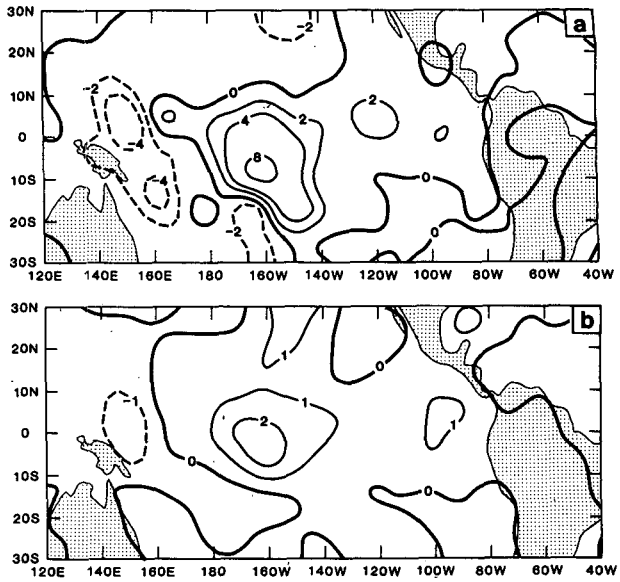

FIG. 7. Average difference $\bar{D}$ between anomaly and control runs for (a) precipitation (mm/day) and (b) evaporation (mm/day).

It is notable that in all cases the major redistribution of precipitation takes place in the western half of the Pacific, as observed, even though the largest SST anomalies are in the eastern half of the Pacific. Evidently, the simulated atmospheric response depends not only upon the position of the anomaly, but also upon the climatological mean SST distribution upon which the anomaly is superimposed. The nature of this dependence is not fully understood. Bjerknes (1969) proposed that increased availability of moisture due to the warmer surface waters near the dateline was primarily responsible for the increase in precipitation in that region during the warm episodes. The change in evaporation (anomaly minus control), averaged for all the experiments shown in Fig. 7b is in the proper sense to contribute to the changes in precipitation: evaporation increases near the dateline where precipitation increases, and it decreases further to the west where the precipitation decreases. However, it is evident that local changes in evaporation can account for only a small fraction of the changes in precipitation in Fig. 7a. Evidently, there are also

systematic changes in the low level circulation which influence the transport of moisture. For a discussion of these changes, see Section 5d.

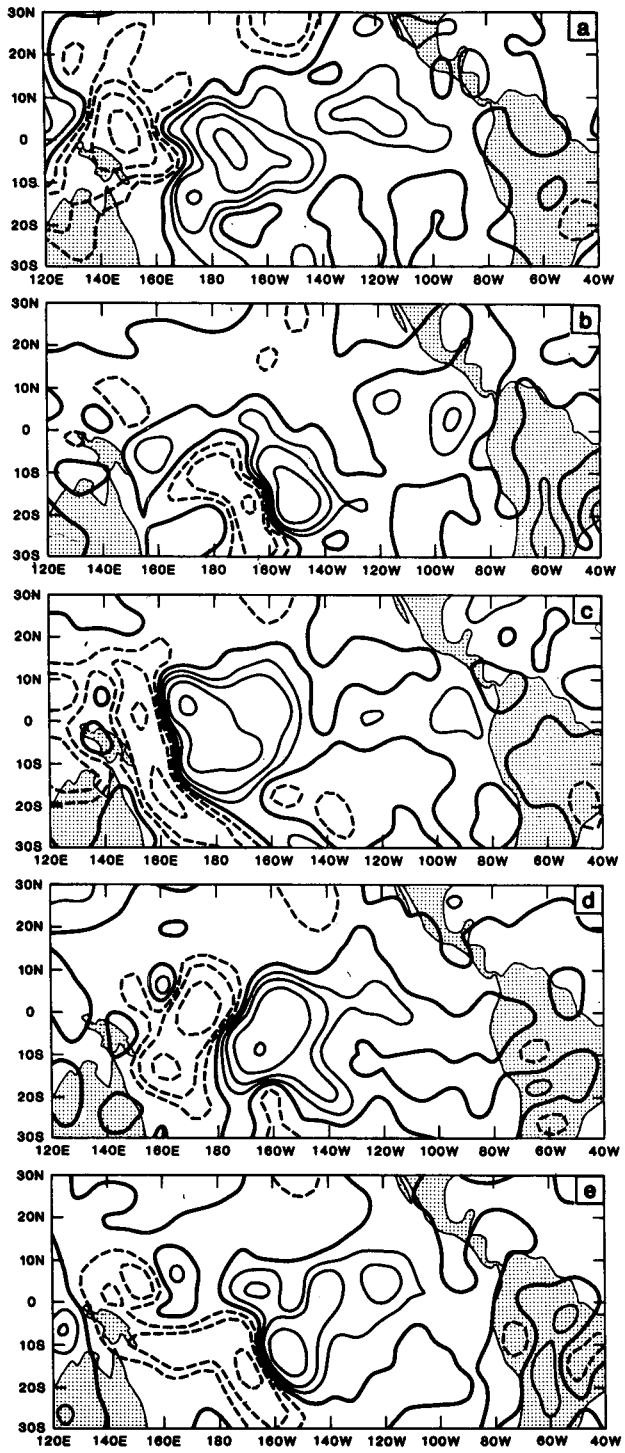

FIG. 8. Precipitation differences between anomaly and control runs for (a) D_{11}, (b) D_{12}, (c) D_{21}, (d) D_{22} and (e) D_{31}. Thick solid contour denotes the zero contour, thin solid and dashed lines denote positive and negative contours respectively with logarithmic contour intervals of 2, 4, 8 and 16 mm day^{-1}.

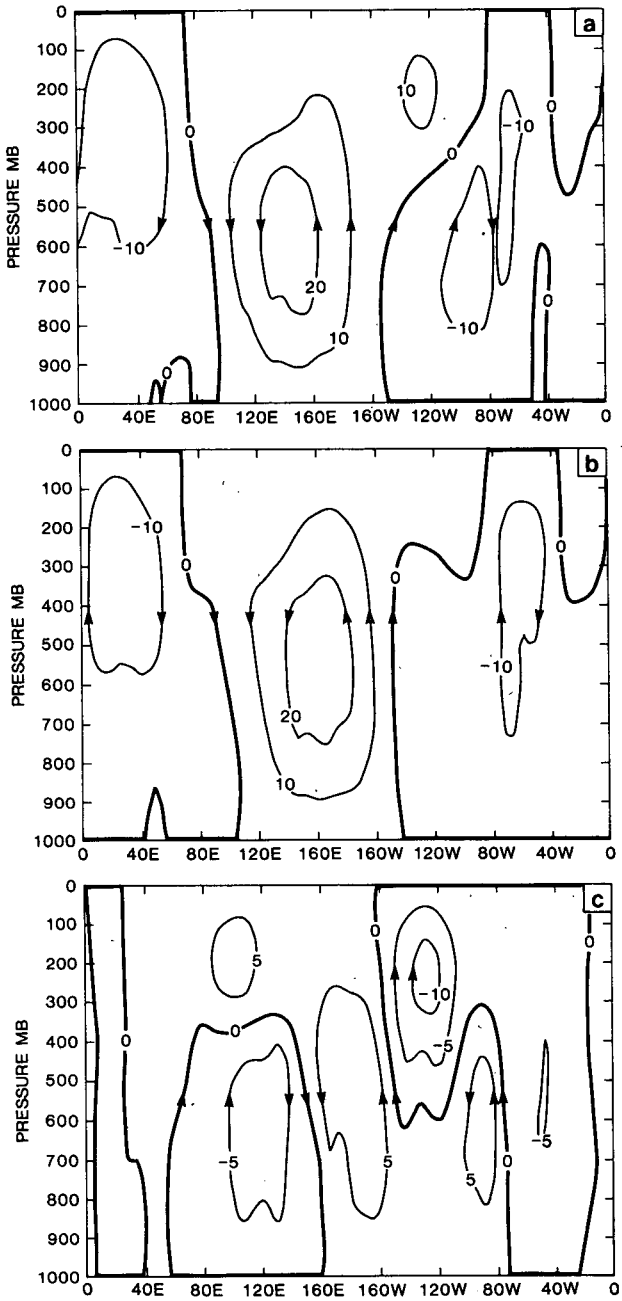

FIG. 9. Streamfunction associated with the Walker circulation averaged between 6°N and 6°S (units of 10^9 kg s^{-1}) for (a) control runs $\bar{C}$, (b) anomaly runs $\bar{A}$ and (c) difference $\bar{D}$.

Fig. 9 shows the long term average control, anomaly and difference streamfunction fields associated with the Walker circulation[2] averaged between 6°N and 6°S. In agreement with the qualitative sugges-

[2] In this study, the Walker circulation was defined by averaging the zonal velocity between 6°N and 6°S as a function of longitude and using this field to construct a stream function in the zonal plane.

tions of Bjerknes (1969), and results of simple models with prescribed heat sources over equator [viz. Gill (1980)], Fig. 9c shows the anomalous Walker cell in the western Pacific with upward motion near 160°W and downward motion near 150°E, which is a reflection of the eastward shift of the rain area. The corresponding changes for the individual five cases, and especially for days 11–25 of first pair of experiments (C_{11}) were much more dramatic. Fig. 10 shows the corresponding results for the zonally averaged Hadley circulation. Although the Hadley circulation with warm SST anomalies for individual cases was found to be a little more intense compared to the control cases, the long term average difference (Fig. 10c) do not exhibit a well defined pattern on the scale of the Hadley circulation. The regionally averaged north–south overturnings over the western Pacific were systematically intensified in the warm SST cases.

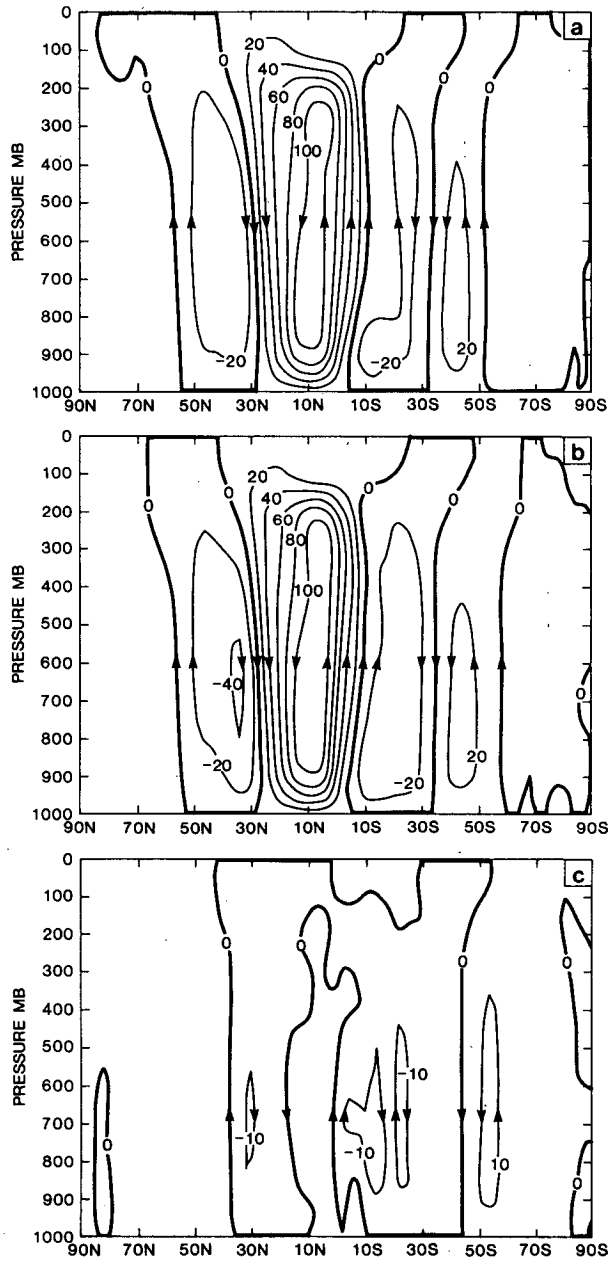

FIG. 10. Hadley circulation (units of 10^9 kg s^{-1}) for (a) control runs $\bar{C}$, (b) anomaly runs $\bar{A}$ and (c) difference $\bar{D}$.

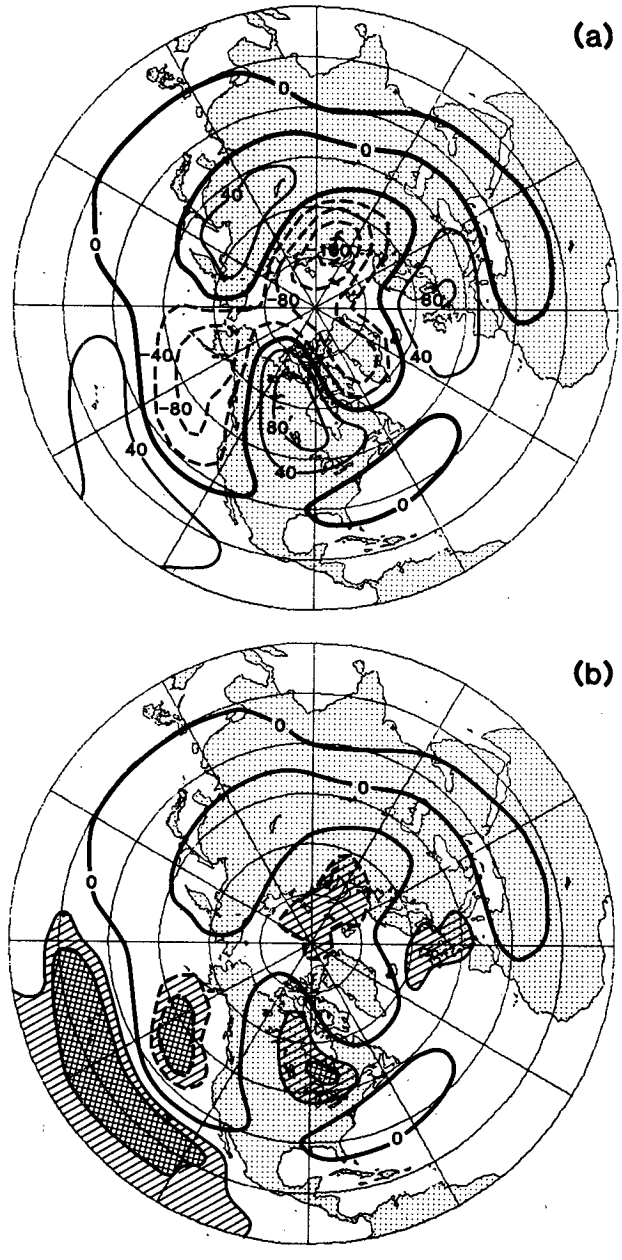

FIG. 11. (a) Average difference $\bar{D}$ for 300 mb height (m) between anomaly and control runs; contour interval 40 m. (b) Areas with t value significant at levels above 95% (dashed) and above 99% (cross hatched) for 300 mb height differences in the five cases D_{11}, D_{12}, D_{21}, D_{22}, D_{31}.

b. *Upper level flow*

The composite pattern of 300 mb height change (anomaly minus control, averaged over the five

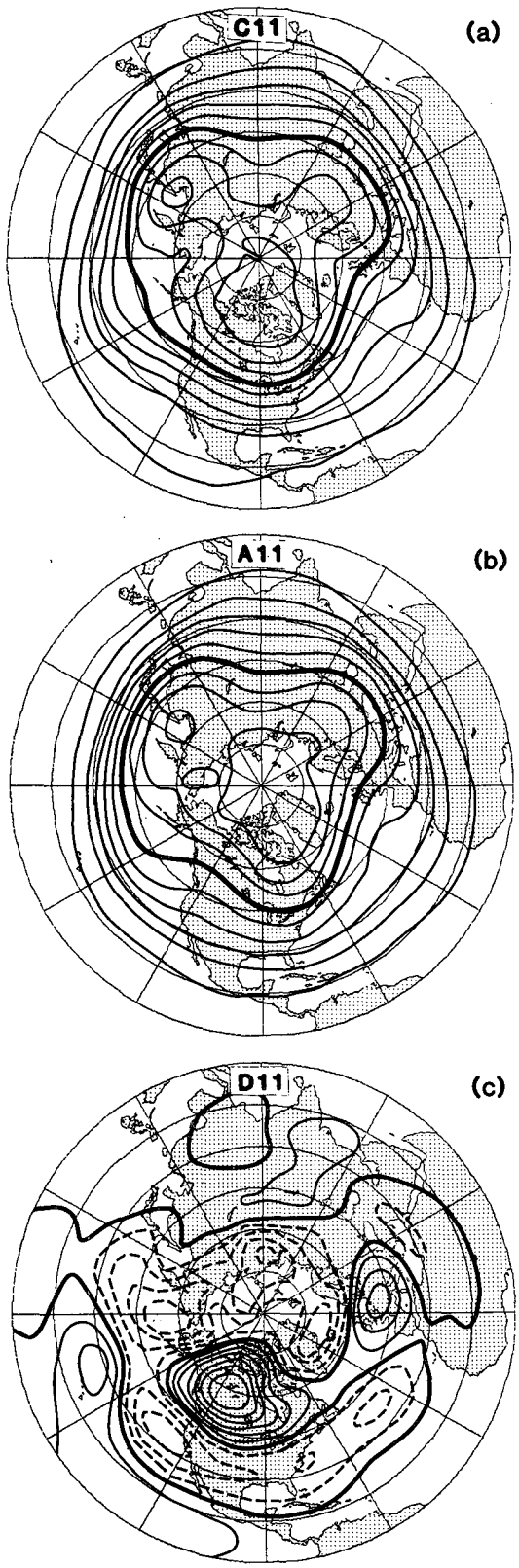

FIG. 12. 300 mb height for (a) control run C_{11}, (b) anomaly run A_{11} and (c) difference D_{11}. In (a) and (b), the thick solid contour denotes the 8930 contour; contour interval 160 m, in (c) the thick solid contour denotes the zero contour, the thin solid and dashed lines denote positive and negative contours, respectively, with contour interval of 40 meters.

months of the experiments) shown in Fig. 11, bears a strong resemblance to the observational pattern depicted schematically in Fig. 3a, which constitutes the *a priori* hypothesis to be tested in these numerical experiments. The wavetrain arching across the North Pacific and North America is in close agreement with the observations with respect to the shape and placement of the centers. The amplitude of this wavetrain is also in reasonably close agreement with composite anomalies presented by Horel (1983). The one disturbing aspect of the pattern in Fig. 11a is the presence of additional features over the northern part of the Eurasian continent, which have no counterpart in the observations. A student *t*-test was performed to assess the significance of the difference between control and anomaly runs for the five month ensemble and the results shown in Fig. 11b show that the differences for the Pacific sector are highly significant while those for other regions may be viewed as indications of the model's natural variability.

An inspection of the height change patterns for individual months (Figs. 12c–16c) provides further evidence concerning the reproducibility of the experimental results. Patterns for all five months show evidence of height increases over the subtropical Pacific, with decreases further to the north, due to the presence of the SST anomalies. Elsewhere the pattern is much more variable from month to month. It is evident that D_{11} is responsible for much of the wavetrain signature over North America in the composite pattern but D_{12}, D_{22} and D_{31} also contribute in the same sense. The features over Eurasia in $\bar{D}$ appear to result mainly from D_{12} and D_{22}. A sample of five months is evidently not large enough to separate all the reproducible features from the spurious ones. However, the pattern over the Pacific sector appears to be quite reproducible in the individual monthly realizations.

It is interesting to note that of the five individual months, the one that shows the strongest wavetrain over the Pacific sector of North America (D_{11}) is also the one that shows the most pronounced east–west redistribution of precipitation in the equatorial Pacific, whereas the ones with the weakest wavetrain were characterized by weak (D_{12}) or longitudinally localized (D_{21}) equatorial precipitation anomalies. The present five month sample is too small to test the statistical significance of this apparent relationship.

It is of interest to consider whether the differences in the 300 mb height field between the respective months of the control and anomaly runs are large enough to have a substantial impact upon the hemispheric circulation pattern. For this purpose, the dif-

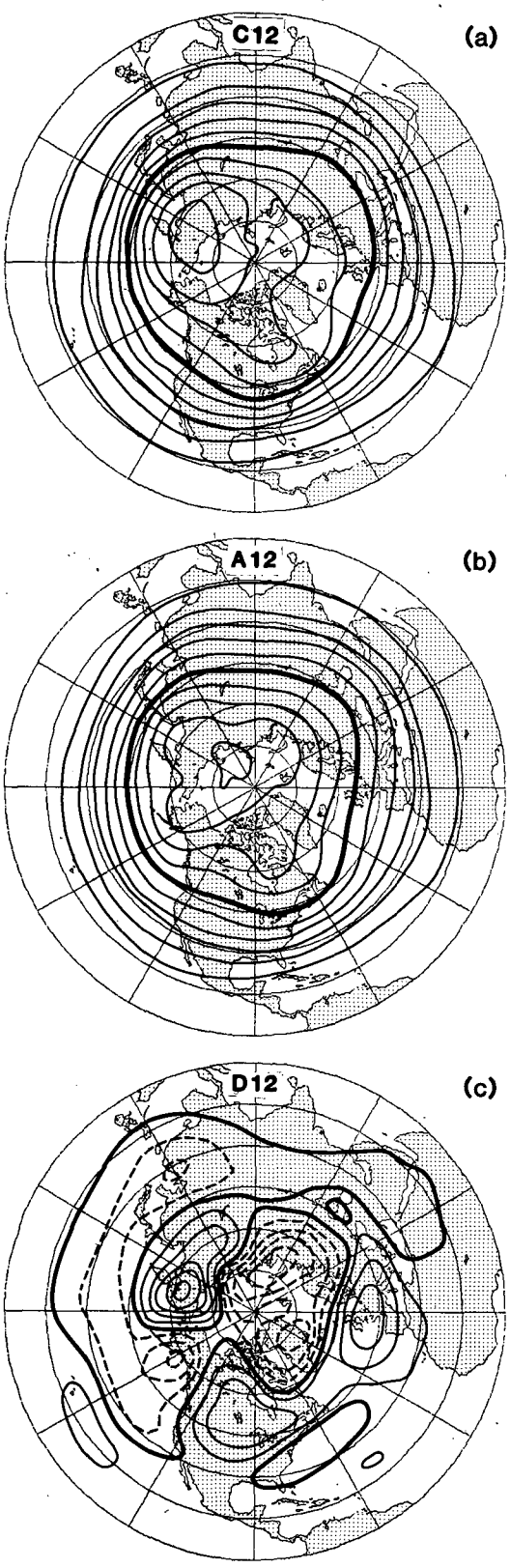

FIG. 13. 300 mb height for (a) control run C_{12}, (b) anomaly run A_{12} and (c) difference D_{12}. Further details as in Fig. 12.

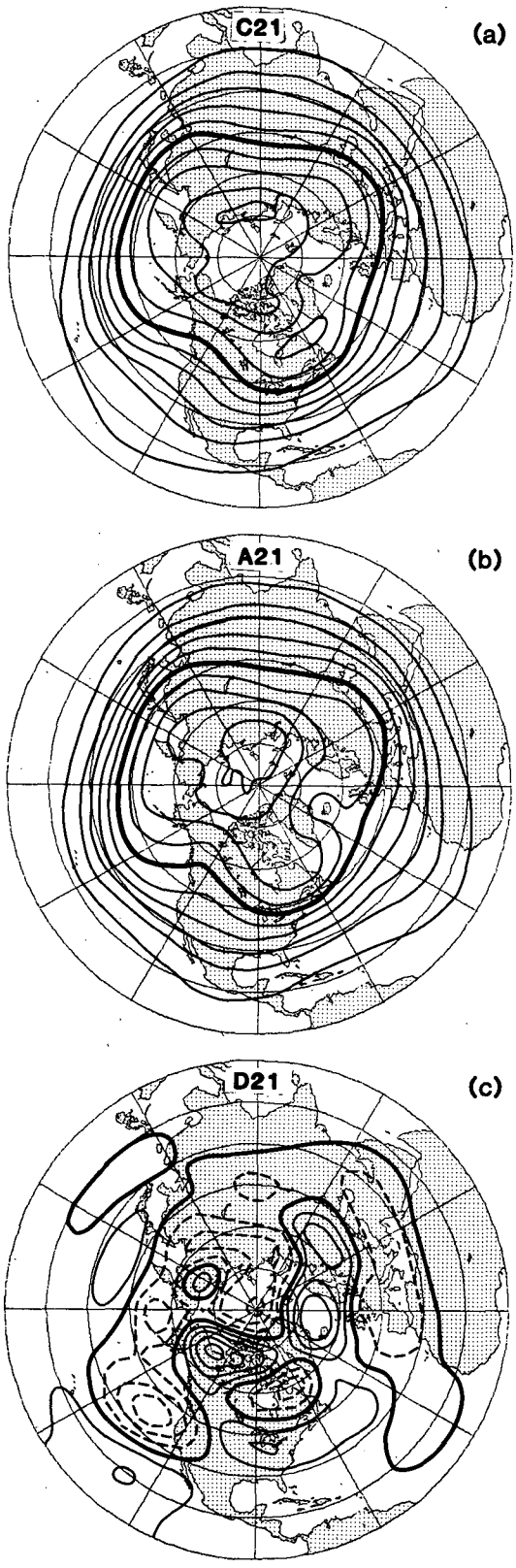

FIG. 14. 300 mb height for (a) control run C_{21}, (b) anomaly run A_{21} and (c) difference D_{21}. Further details as in Fig. 12.

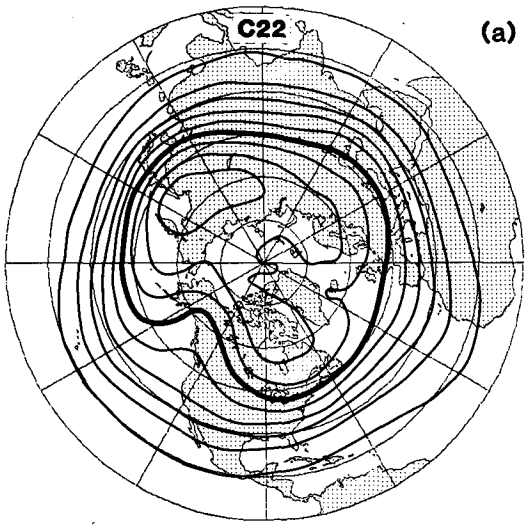

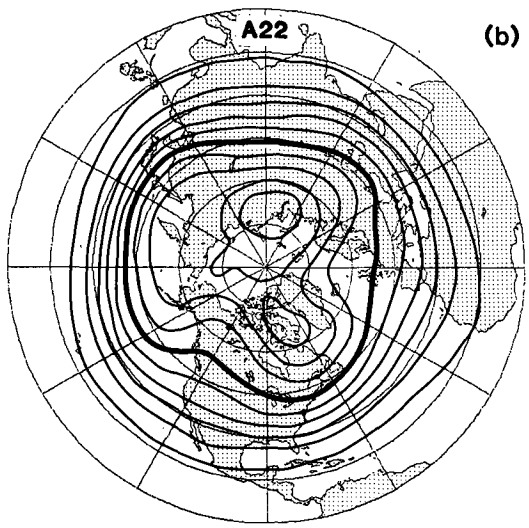

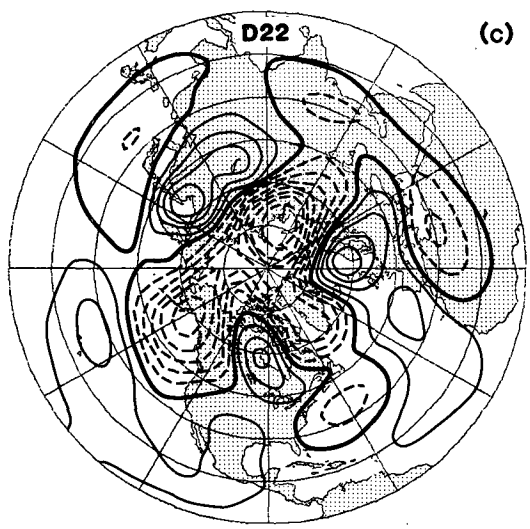

FIG. 15. 300 mb height for (a) control run C_{22}, (b) anomaly run A_{22} and (c) difference D_{22}. Further details as in Fig. 12.

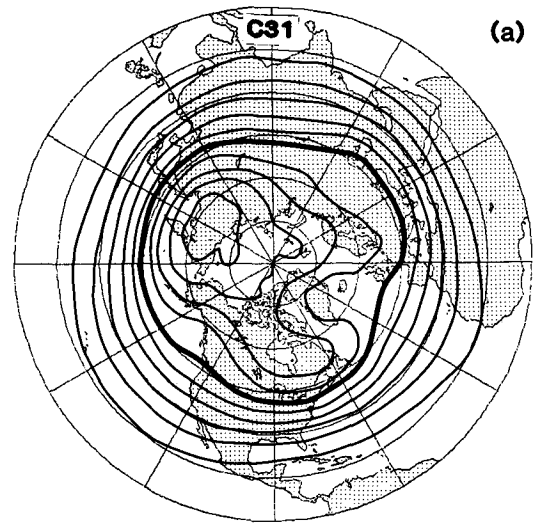

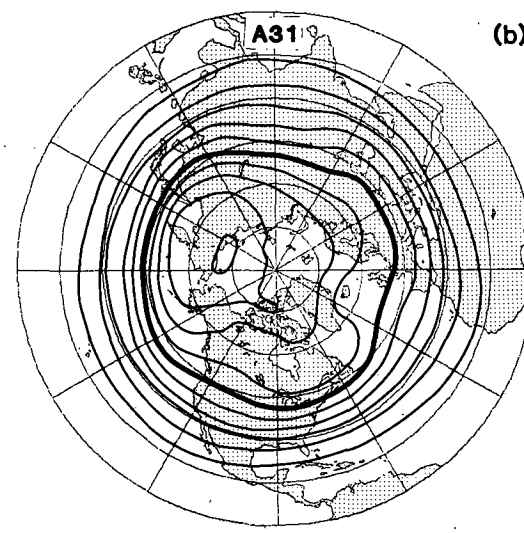

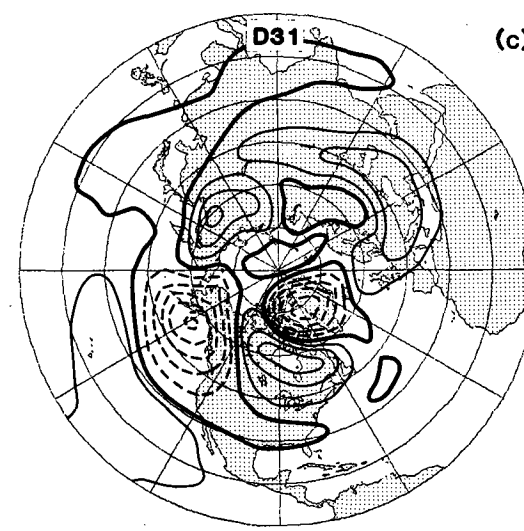

FIG. 16. 300 mb height for (a) control run C_{31}, (b) anomaly run A_{31} and (c) difference D_{31}. Further details as in Fig. 12.

ference maps in Figs. 12–16 are shown together with the respective control run and anomaly run maps. In the first month of the first experiment (Fig. 12) the differences between control and anomaly experiments over the Pacific and North American sectors are large enough to be reflected in the circulation patterns; the flow in control run is much more zonal over western Canada and the northwestern United States than in the anomaly run and the circulation over the Gulf of Alaska is more cyclonic. The differences in the second month of the run (Fig. 13) are more subtle over the region of primary interest but there are pronounced differences over the Siberian Arctic which are mirrored in the patterns for the second month of the second experiment (Fig. 15). Both months of the second experiment are characterized by strong ridges positioned near the west coast of Canada in both anomaly runs and control runs. The month to month differences between control (or anomaly) runs are comparable to the differences be-

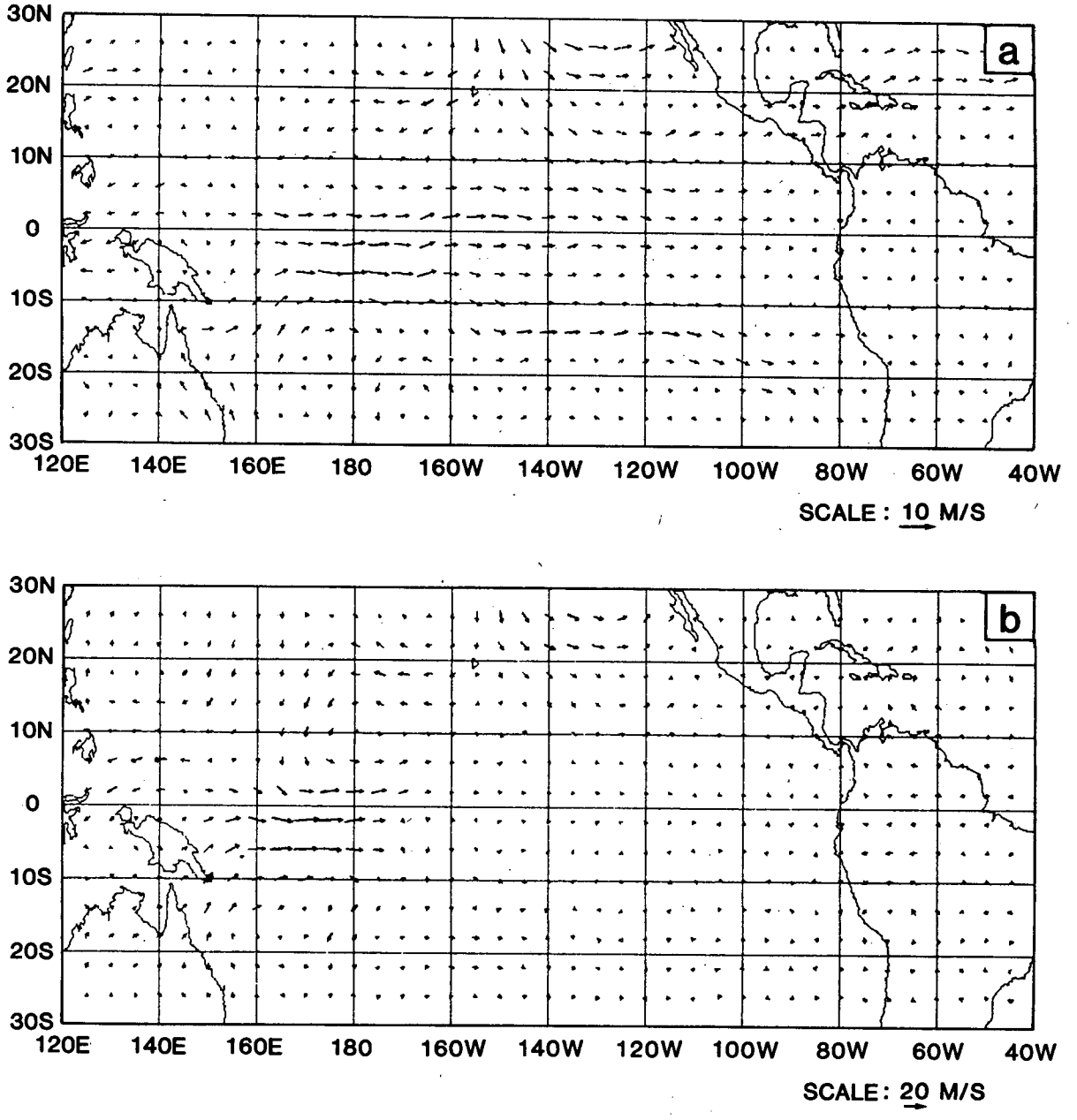

FIG. 17. Vector wind difference at 700 mb between anomaly and control runs: (a) average difference $\bar{D}$, (b) for averaging period corresponding to days 11–25 of C_{11} and A_{11}. Lengths of arrows denote the wind speed according to the scale at the bottom.

tween the respective control and anomaly runs over the North American sector.

c. *Low-level circulation and temperature*

Fig. 17 shows the composite difference between the low-level (700 mb) circulation in the three anomaly experiments and the corresponding circulation in the respective control experiments. (The 700 mb level was selected here to represent the low level circulation because the surface wind is only an extrapolated field in the GLAS model.) The most prominent feature in this pattern is the increase in the westerlies along the equator just to the west of the dateline. This change is in qualitative agreement with the observational picture (Fig. 3b) and with theoretical evidence based on simpler models. The magnitudes of the changes appear to be larger than those for observations at 850 mb (Horel, personal communication, 1983). There is also some tendency for an increase in the strength of the tradewinds along 15–20°N in the western Pacific, but it is not as widespread as in the surface wind observations. The corresponding distribution for days 11–25 of the first experiment, shown in Fig. 17b, exhibits a similar but stronger pattern (note the scales at the bottom of the figure).

The increase in low level westerlies to the west of the dateline plays the leading role in accounting for the changes in the moisture budget associated with the eastward shift of precipitation which occurs in response to the SST anomalies. This anomalous westerly flow carries moisture out of the region where the heavy precipitation occurs in the control experiments and deposits it in the region of heavy rainfall of the anomaly experiments.

The corresponding changes in the sea-level pressure (SLP) patterns, shown in Fig. 18, are in reasonably good agreement with the observational picture in Fig. 3b to the extent that they can be compared. The Southern Oscillation signature is manifested in the higher SLP over Australia and the subtropical northwest Pacific and the lower SLP over most of the south Pacific, eastward of 150°E. The pattern of SLP changes at higher latitudes (not shown) resembles the pattern of 300 mb height changes.

The pattern of 850–300 mb thickness changes (not shown) also resembles the pattern of 300 mb height changes, as it does in the observations. For D_{11}, the changes over western Canada are equivalent to temperature increases of 4–5°C. Rowntree (1972) also noted large temperature increases in this region. In agreement with the observations and results of earlier

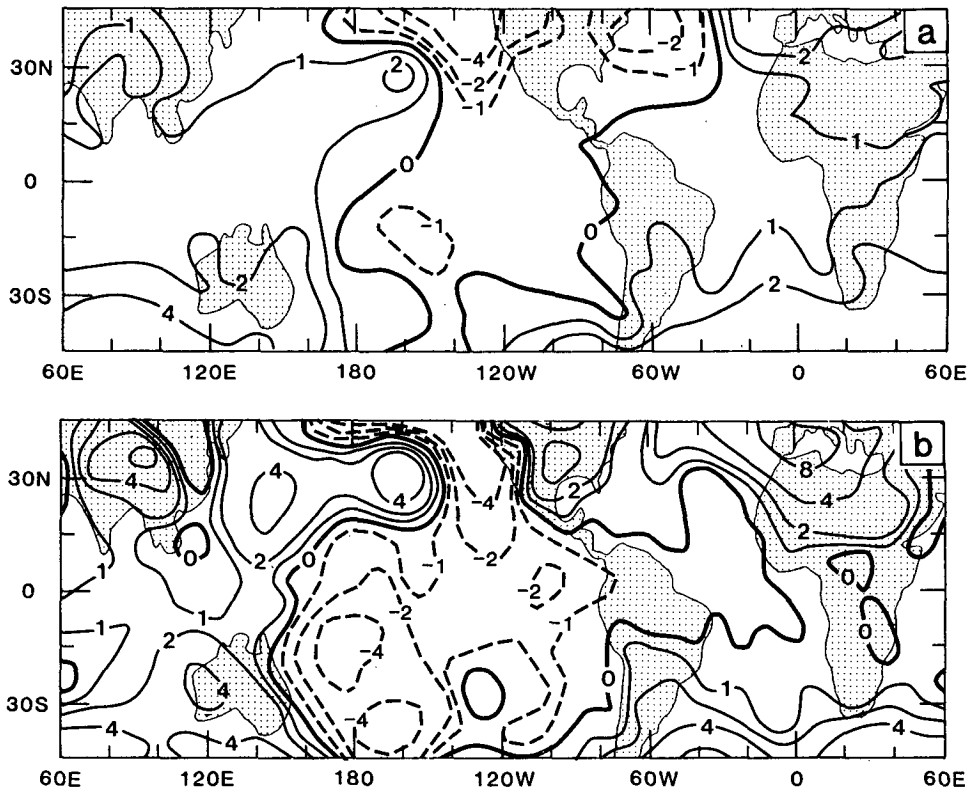

FIG. 18. Sea level pressure (mb) difference between anomaly and control runs: (a) average difference $\bar{D}$, (b) for averaging period corresponding to days 11–25 of C_{11} and A_{11}.

works using simple models and GCMs, the simulated circulation anomalies in the tropics exhibit a monsoon like vertical structure with perturbations of opposite polarity in upper and lower troposphere, and a simpler vertical structure in the middle latitudes with height and wind anomalies being in phase at all levels.

d. Tropical tropospheric temperature

Time series of 1000–200 mb thickness, averaged for the latitude belt from 30°N to 30°S were generated in order to determine whether the presence of the SST anomalies contributed to a general warming of the tropical troposphere, in agreement with observational results of Angell and Korshover (1978), Newell (1979), and Horel and Wallace (1981). Results for the first experiment, shown in Fig. 19, show existence of a marked upward trend in tropical tropospheric temperature in both the control run and the anomaly run. Similar upward trends occurred in the other experiments. These trends are apparently a reflection of the fact that the equilibrium tropical tropospheric temperatures in the GLAS model are warmer, by ~5 K than the observed temperatures that are imposed on the model in the initial conditions. By the end of the first month of the integrations, the model has accomplished most of the adjustment to its own equilibrium temperatures, but some further drift occurs during the second month. Because of this pronounced "climate drift" problem of the GLAS model, we are reluctant to attribute much significance to the results of Fig. 19 which show a warmer tropical troposphere in the anomaly run compared to the control run.

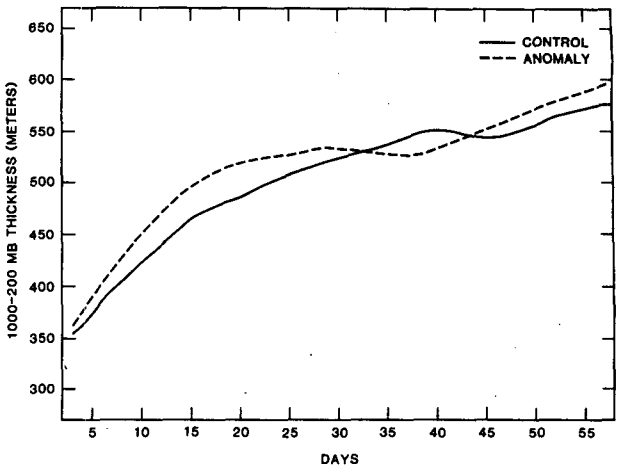

FIG. 19. Time series of 1000–200 mb thickness (m) for control run C_1 (solid line) and anomaly run A_1 (dashed line).

6. Discussion and concluding remarks

In parallel with the discussion in Section 2, it is possible to assess the results of our experiments from two different vantage points: 1) without the benefit of prior modeling experience or any specific *a priori* hypothesis concerning dynamical mechanisms beyond the conceptual model of Bjerknes (1969), and 2) in light of the hypothetical dynamical framework described in Section 1 and the experience acquired from previous GCM investigations.

1) Our results concerning the redistribution of precipitation within the equatorial belt and the changes in the 300 mb height field in the Pacific sector are sufficiently consistent from one month of the experiments to another to give a reasonably definitive qualitative indication of how the model responds to the prescribed SST anomalies. The sense and magnitude of the model response are such as to support Bjerknes' view that much of the observed interannual variability in the Pacific sector can be interpreted as a response to equatorial SST anomalies. The 300 mb height changes in other sectors of the Northern Hemisphere appear to be less reproducible in our experimental results.

Without the benefit of *a priori* knowledge, the only basis to attach more significance to the changes over North America than to those over the Eurasian continent would have been the statistical *t*-test whose validity can be questioned due to inherent spatial autocorrelations of the height field.

2) The degree of confidence that can be attached to our results for the Pacific sector is considerably enhanced by the knowledge that other investigators have obtained similar results and by the existence of a dynamical framework for interpreting the response. (Conversely, these new experimental results can be viewed as confirming the results of previous GCM studies, and as providing evidence for validating the dynamical interpretations derived from the simpler, more idealized models.) From this second vantage point it is tempting to regard the response in the 300 mb height field over North America as a partially successful simulation of the observational results in Fig. 3a, though this particular aspect of the results cannot be regarded as definitive. It is perhaps encouraging that the experimental month with the most clearly defined signal in the tropical rainfall distribution was also the month with the largest 300 mb height anomalies over the North Pacific and North America.

Our experiments are subject to at least three serious limitations, which prevent us from making more definitive statements concerning the atmospheric response to equatorial SST anomalies:

1) As pointed out in Section 5e, the temperature of the model tropics becomes considerably warmer than the observed temperature after the first few

weeks of the integrations. This climate drift problem could conceivably render the model less sensitive to SST anomalies than it should be or it could distort the model response.

2) The model integrations were carried out with one particular choice of boundary layer and convective parameterization schemes. It is conceivable that other choices might have led to somewhat different results. On the other hand, it could be argued that for any reasonable boundary layer parameterization scheme, the atmospheric surface temperature should never depart very much from the imposed sea-surface temperature and for any reasonable convective parameterization scheme, tropospheric lapse rates should never depart very far from moist adiabatic; hence the manner in which the horizontal pattern of sea-surface temperature differences between control and anomaly runs is reflected in the deep tropospheric temperature field might not prove to be particularly sensitive to the details of the parameterization schemes.

3) As pointed out by Rowntree (1972, 1976) the results for extratropical latitudes exhibit a considerable amount of sampling variability from one experiment to another and from one month (or other sampling period) to another within a given experiment. The five months of integrations carried out in this study does not, in our opinion, constitute a sufficient sample size to permit an accurate and comprehensive determination of the extratropical response to equatorial SST anomalies. The same limitation applies to the previous GCM studies discussed in Section 2.

The need for longer (and/or more numerous) numerical integrations transcends the issue of signal-to-noise ratio discussed by Leith (1973). It is clear that the atmosphere itself is capable of exhibiting a wide range of behavior in monthly or seasonal mean statistics. For example, the wavetrain over North America in Fig. 3a was strongly developed during the two winters of the 1976–78 warm SST episode in the equatorial Pacific but it was largely absent during the even stronger 1972–73 warm episode; the wavetrain was present for three continuous weeks during January 1981 which did not fall within a warm episode. Likewise, extended GCM integrations exhibit a considerable amount of month-to-month and interannual variability, even in the absence of SST anomalies [Lau (1981)]. Therefore, a complete and reproducible documentation of model response will probably require at least an order of magnitude larger sample than the five simulated months which form the basis of this study. It has recently come to our attention that Blackmon *et al.* (1983) have carried out a similar numerical experiment using similar SST anomalies by integrating the NCAR model for 1200 days in perpetual January mode.

The methodology for analyzing the results of such extensive sets of sensitivity experiments has only recently begun to be explored. It is clear that ensemble averages for perturbed and unperturbed states such as those presented in Fig. 3 give only the most rudimentary description of the sensitivity; a more complete description would include changes in the frequency and duration of various circulation regimes between the model climatologies for the perturbed and unperturbed states. The proper design and analysis of such extensive sets of sensitivity experiments will require a better understanding of the nature and causes of low-frequency atmospheric variability.

Finally, based on the results of short period averages (days 11–25) some general remarks can be made regarding the use of this or similar GCMs for dynamical prediction of monthly and seasonal means. The present results suggest that the dynamical prediction of monthly means for even first 30 days with climatological mean boundary conditions of sea surface temperature can be significantly different from those with the observed SST during that month, and therefore the problem of specifying boundary conditions of SST over equatorial Pacific (or more generally, the global boundary conditions of SST, soil moisture and snow/sea ice, etc.) should be studied in greater detail.

Acknowledgments. We wish to thank Mr. Mike Fennessy for processing a large number of model output tapes and performing most of the calculations; Eugene M. Rasmusson and T. Carpenter for supplying the SST anomaly data; Laura Rumburg for drafting work; and Mary Ann Schaefer for typing the manuscript.

REFERENCES

Angell, J. K., and J. Korshover, 1978: Estimate of global temperature variations in the 100–30 mb layer between 1958 and 1977. *Mon. Wea. Rev.*, **106**, 1422–1432.

Barnett, T. P., 1977: An attempt to verify some theories of El Niño. *J. Phys. Oceanogr.*, **7**, 633–647.

Bjerknes, J., 1969: Atmospheric teleconnections from the equatorial Pacific. *Mon. Wea. Rev.*, **97**, 162–172.

Blackmon, M. L., J. E. Geisler and E. J. Pitcher, 1983: A general circulation model study of January climate anomaly patterns associated with interannual variation of equatorial Pacific sea surface temperatures. *J. Atmos. Sci.*, **40**, 1410–1425.

Doberitz, R., 1968: Cross spectrum analysis of rainfall and sea temperature at the equatorial Pacific Ocean. *Bonn. Meteor. Abh.*, **8**, 61 pp.

Gill, A. E., 1980: Some simple solutions for heat-induced tropical circulation. *Quart. J. Roy. Meteor. Soc.*, **106**, 447–462.

Heddinghaus, T. R., and A. F. Krueger, 1981: Annual and interannual variations in outgoing longwave radiation over the tropics. *Mon. Wea. Rev.*, **109**, 1208–1218.

Horel, J. D., 1983: Interannual variation of rainfall, geopotential height and wind associated with the Southern Oscillation. Submitted to *Mon. Wea. Rev.*

——, and J. M. Wallace, 1981: Planetary scale atmospheric phenomena associated with the Southern Oscillation. *Mon. Wea. Rev.*, **109**, 813–829.

Hoskins, B. J., 1983: Dynamical processes in the atmosphere and the use of models. *Quart. J. Roy. Meteor. Soc.* **109**, 1–21.

——, and D. Karoly, 1981: The steady, linear response of a spherical atmosphere to thermal and orographic forcing. *J. Atmos. Sci.*, **38**, 1179–1196.

——, A. J. Simmons, and D. G. Andrews, 1977: Energy dispersion in a barotropic atmosphere. *Quart. J. Roy. Meteor. Soc.*, **103,** 553–567.

Julian, P. R., and R. M. Chervin, 1978: A study of the Southern Oscillation and Walker circulation phenomenon. *Mon. Wea. Rev.*, **106,** 1433–1451.

Keshavamurty, R. N., 1982: Response of the atmosphere to sea surface temperature anomalies over the equatorial Pacific and the teleconnections of the Southern Oscillation. *J. Atmos. Sci.*, **39,** 1241–1259.

Kidson, J. W., 1975: Tropical eigenvector analysis and the Southern Oscillation. *Mon. Wea. Rev.*, **103,** 187–196.

Lau, N. C., 1981: A diagnostic study of recurrent meteorological anomalies appearing in a 15-year simulation with a GFDL general circulation model. *Mon. Wea. Rev.*, **109,** 2287–2311.

Lau, K. M., and P. H. Chan, 1983: Short-term climate variability and atmospheric teleconnections from satellite observed outgoing longwave radiation. *J. Atmos. Sci.* (in press).

Leith, C. E., 1973: The standard error of time-averaged estimates of climatic means. *J. Appl. Meteor.*, **12,** 1066–1069.

Liebmann, B., and D. L. Hartmann, 1982: Interannual variation of outgoing IR in association with tropical circulation changes during 1974–78. *Mon. Wea. Rev.*, **39,** 1153–1162.

Matsuno, T., 1966: Quasi-geostrophic motions in the equatorial area. *J. Meteor. Soc. Japan, Ser. II,* **44,** 25–43.

Moura, A. D., and J. Shukla, 1981: On the dynamics of droughts in northeast Brazil: Observations, theory, and numerical experiments with a general circulation model. *J. Atmos. Sci.*, **38,** 2653–2675.

Newell, R. E., 1979: Climate and the ocean. *Amer. Sci.*, **67,** 405–416.

Opsteegh, J. D., and H. M. van den Dool, 1980: Seasonal differences in the stationary response of a linearized primitive equation model: Prospects for long range forecasting? *J. Atmos. Sci.*, **37,** 2169–2185.

Pittock, A. B., 1973: Global meridional interactions in the stratosphere and troposphere. *Quart. J. Roy. Meteor. Soc.*, **99,** 424–437.

Quinn, R. W., D. O. Zopf, K. S. Short and R. T. W. Kuo-Yang, 1978: Historical trends and statistics of the Southern Oscillation, El Niño and Indonesian droughts. *Fish. Bull.*, **76,** 663–678.

Rao, M. S. V., and J. Theon, 1977: New features of global climatology revealed by satellite-derived oceanic rainfall maps. *Bull. Amer. Meteor. Soc.*, **58,** 1285–1288.

Rasmusson, E., and T. Carpenter, 1982: Variations in tropical sea surface temperature and surface wind fields associated with the Southern Oscillation/El Niño. *Mon. Wea. Rev.*, **110,** 354–384.

Rowntree, P. R., 1972: The influence of tropical east Pacific Ocean temperatures on the atmosphere. *Quart. J. Roy. Meteor. Soc.*, **98,** 290–321.

——, 1976: Response of the atmosphere to a tropical Atlantic Ocean temperature anomaly. *Quart. J. Roy. Meteor. Soc.*, **102,** 607–625.

Shukla, J., 1975: Effect of Arabian sea-surface temperature anomaly on the Indian summer monsoon: A numerical experiment with GFDL model. *J. Atmos. Sci.*, **32,** 503–511.

——, D. Straus, D. Randall, Y. Sud and L. Marx, 1981: Winter and summer simulations with the GLAS climate model. NASA Tech. Memo. 83866, 282 pp. [NTIS N8218807].

Simmons, A. J., Wallace, J. M. and G. W. Branstator, 1983: Barotropic wave propagation and instability, and atmospheric teleconnection patterns. *J. Atmos. Sci.*, **40,** 1363–1392.

Webster, P. J., 1981: Mechanisms determining the atmospheric response to sea surface temperature anomalies. *J. Atmos. Sci.*, **38,** 554–571.

——, 1982: Seasonality in the local and remote atmospheric response to sea surface temperature anomalies. *J. Atmos. Sci.*, **39,** 41–52.